Characterizing and Modeling the Noise and Complex Impedance of Feedhorn-Coupled TES Polarimeters

J.W. Appel[*], J. E. Austermann[†], J.A. Beall[**], D. Becker[**], B.A. Benson[‡], L.E. Bleem[‡], J.Britton[**], C. L. Chang[‡], J.E. Carlstrom[‡], H.M. Cho[**], A.T. Crites[‡], T. Essinger-Hileman[*], W. Everett[‡], N.W. Halverson[†], J.W. Henning[†], G.C. Hilton[**], K.D. Irwin[**], J. McMahon[‡], J. Mehl[‡], S.S. Meyer[‡], M.D. Niemack[**], L.P. Parker[*], S.M. Simon[†], S. T. Staggs[*], C. Visnjic[*], K.W. Yoon[**] and Y. Zhao[*]

[*] *Joseph Henry Laboratories of Physics, Jadwin Hall, Princeton University, Princeton, NJ, 08544, USA*
[†] *Center for Astrophysics and Space Astronomy, Department of Astrophysical and Planetary Sciences and Department of Physics, University of Colorado, Boulder, CO 80309, USA*
[**] *NIST Quantum Devices Group, 325 Broadway Mailcode 817.03, Boulder,CO, USA 80305, USA*
[‡] *Kavli Institute for Cosmological Physics, University of Chicago, 5640 South Ellis Avenue, Chicago, IL 60637, USA*

Abstract. We present results from modeling the electrothermal performance of feedhorn-coupled transition edge sensor (TES) polarimeters under development for use in cosmic microwave background (CMB) polarization experiments. Each polarimeter couples radiation from a corrugated feedhorn through a planar orthomode transducer, which transmits power from orthogonal polarization modes to two TES bolometers. We model our TES with two- and three-block thermal architectures. We fit the complex impedance data at multiple points in the TES transition. From the fits, we predict the noise spectra. We present comparisons of these predictions to the data for two TESes on a prototype polarimeter.

Keywords: cmb, polarimeter, TES
PACS: 95.85.Bh,95.75.Hi,95.55.Rg,95.55.Qf,07.57.Kp

INTRODUCTION

We have constructed two models for the transition edge sensor (TES) used in the feedhorn-coupled TES polarimeters []. The models describe the electrical and thermal behavior of the TESes. One of the models has a two block thermal architecture and the other uses three blocks. Their parameters are determined from *I-V* curves, Johnson noise data, and measurements of the complex impedance, $Z(\omega)$ at three points in the TES transition. Each setpoint is described by the mean current I_0 through the TES and its resistance R_0. The noise spectra predicted from these models agree well with the measured noise from a few Hz to many kHz after addition of a single free parameter at each setpoint to account for excess Johnson noise. Both models require larger heat capacities than predicted from initial estimates based on the materials found on the TES island. We compare results from two separate TESes, finding good agreement in the parameter estimates from the complex impedance fit.

TES MODELS

A simple TES model such as that described in [1], for example, predicts that $Z(\omega)$ will trace out a semicircle in the complex plane. The TES bolometers described here do not exhibit semicircular $Z(\omega)$, suggesting that they have a complex thermal architecture similar to those described in [2], [3], for example. The TES islands of these bolometers comprise SiO_2 and SiN layers, a Nb ground plane, a lossy gold microstrip as the microwave absorber, a gold heater resistor, and a MoCu TES. (See for example Fig X from Ki Won?). Initial estimates for the heat capacities of the different components from their bulk properties are given in Table 1. Note that the TES itself only accounts for 15% of the initial estimate, motivating inclusion of an extra heat capacity between the TES and the bath in the model.

The two architectures we consider here are found in Figure 1. In each, a block of heat capacity C_1 is thermally connected to the bath by a thermal conductivity G_{bath}, a heat capacity C_2 is connected to C_1 through a conductivity G_2 and the electrical bias power is dissipated in C_2. In the three-block model, an additional 'hanging' heat capacity C_3 is connected to C_1 through a conductivity G_3.

Here we do not provide identification of each block

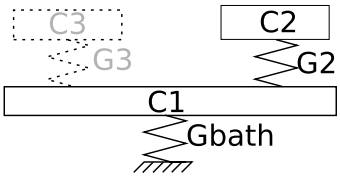

FIGURE 1. The diagram shows the thermal architecture of the two- and three-block models used to fit $Z(\omega)$. In both models, the bias power is dissipated on C_2. In the two-block model G_3 and C_3 do not exist.

TABLE 1. The bulk heat capacities of the pure elements are estimated by adding their electron and phonon heat capacities [4]. The phonon heat capacities are calculated following the Debye model. Note that Nb has no electrical heat capacity because it is a superconductor at 500 mK. The low temperature bulk heat capacities of SiN and $Si0_2$ are found in [5], and [6] respectively.

Material	Location	Volume (μm^3)	Heat Capacity (pJ/K)
Au	microstrip	1530	0.063
Nb	microstrip	1590	0.002
Nb	ground plane	14860	0.016
Mo	TES	699	0.008
Cu	TES	1078	0.054
Cu	TES Bank	748	0.037
SiO_2	Substrate	45750	0.083
SiO_2	Substrate	32025	0.058
SiN	Substrate	45750	0.091
Total			0.412

with a specific component of the bolometer; instead we seek to show that inclusion of additional thermal blocks improves not only the fits to $Z(\omega)$ but also the predictions of the noise spectra. We also considered an alternative two-block model in which the TES and its electrical power were identified with C_1. The fits to $Z(\omega)$ did not improve with that model so we discarded it in favor of the three-block model for comparisons.

FITTING THE DATA

The TES models are expressed in matrix form following [3]. Least squares minimization is used to find the best fit parameter values from the $Z(\omega)$ data at three setpoints simultaneously, via direct numerical solution of the matrix equation at each frequency. The data described here consist of sets of complex impedance data and noise spectra at $R_0 = 0.10R_N$, $0.50R_N$, and $0.90R_N$, where $R_N \approx 5$ mΩ is the normal resistance of the TES. Exploring the extreme ends of the transition is important for lessening parameter degeneracies. Data sets were taken with the bath temperature at $T_{bath} = 0.320$ K; results from $T_{bath} = 0.480$ K agree well.

Each of the two models includes nine fixed parameters from external measurements. These include: the shunt resistance R_{sh} and series inductance L obtained from spectra of the Johnson noise with the TES superconducting; three values each of I_0 and R_0 obtained from I-V curves; and G, the thermal conductivity from the TES to the bath, obtained from I-V curves at multiple values of T_{bath}. (Note that for both models $1/G = 1/G_3 + 1/G_{bath}$.) These parameters are listed above the midline in Table 2.

In linear theory, at each bias setpoint the TES circuit is characterized with two parameters, the logarithmic current derivative $\beta \equiv d\ln(R)/d\ln(I)$, and the loop gain, L_g. The latter is defined by

$$L_g \equiv \frac{(I_0^2 R_0)\alpha}{GT_0}; \qquad \alpha \equiv \frac{d\ln(R)}{d\ln T} = \left(\frac{T}{R}\right)\frac{dR}{dT},$$

where $T_0 \approx T_c$ is the TES temperature. Each of the two models fits for these two parameters at each of the three set points, as well as for C_1, C_2 and G_2. The three-block model also fits for C_3 and G_3. In total there are nine free parameters for the two-block model, and eleven for the three-block model.

The least squares minimization is speeded by initial parameter estimates. We estimate each β from the high frequency data (here at ≈ 40 kHz), where $Z \approx R_0(1+\beta)$. For L_g we examine $Z(\omega \approx 0) \approx (1+\beta+L_g)/(1-L_g)$.

PREDICTING THE NOISE SPECTRA

Having estimated the free parameters of the two models from the $Z(\omega)$ data, we can now predict the noise spectra. The two-block model has four noise sources: Johnson noise from the TES and from the shunt, and thermal phonon noise from G_{bath} and G_2. (We neglect amplifier noise since it is three orders of magnitude lower than the current noise when the TES is normal.) The three-block model has an additional noise term from G_3.

The spectral density of the thermal noise from a conductivity G_i at temperature T is given by Equation 1, where k_B is the Boltzmann constant [7]. The factor $F_{link,i}$ is between 0.5 and 1, depending on the temperature gradient across G_i and the details of the heat transfer (specular or diffuse). Here we neglect the small thermal gradients across the internal G_i, approximating the temperature of each of the blocks as T_c, the critical temperature of the TES. This simplification means that $F_{link,i}$ for all internal connections is unity. For the connection to the bath, we assume the heat transfer is specular so that we can estimate F_{link} from Equation 2, where $n = 2.7$ is the exponent governing power transfer from the TES to the bath, and here we have evaluated it for $T_c = 0.5$ K and $T_{bath} = 0.32$ K.

TABLE 2. This table contains the parameters used in and resulting from fits to $Z(\omega)$ data for TESA and TESB on one feedhorn-coupled polarimeter. It also estimates the NEP at 10 Hz of each TES, as described in the text. The superscripts *h*, *m*, and *l* label parameters with R_o at 90%, 50%, and 10% of R_n respectively. The parameters above the midline comes from *I-V* curves and Johnson noise. Those below the line are from the two-block model fits. The estimated error on the shunt value is 5%, this error propagates to all other set parameters. Using the bootstrap method we estimate the error on β, and L_g to be at the 5% level while the error on C_1, C_2 and G_2 is around 25%.

	TESA	**TESB**
T_o	0.50	0.50
R_{sh} (mΩ)	0.18	0.18
L (nH)	33	34
R_N (mΩ)	5.2	5.3
R_o^h (mΩ)	4.7	4.7
R_o^m (mΩ)	2.6	2.6
R_o^l (mΩ)	0.5	0.5
I_o^h (mA)	0.05	0.05
I_o^m (mA)	0.06	0.06
I_o^l (mA)	0.13	0.16
G (pW/K)	80	79
C_1 (pJ/K)	1.8	1.6
C_2 (pJ/K)	0.7	0.8
G_2 (pW/K)	2700	2300
L_g^h [α^h]	4[14]	4[15]
L_g^m [α^m]	13[56]	16[67]
L_g^l [α^l]	49[241]	39[210]
β^h	0.1	0.1
β^m	0.9	1.4
β^l	9.0	8.4
J_{excess}^h	1.1	1.6
J_{excess}^m	8.1	20
J_{excess}^l	50	237
NEP_{10Hz} (W/$\sqrt{Hz}$)	3.3e-17	3.5e-17

$$SD_i = 4F_{link,i}k_B G_i T^2. \quad (1)$$

$$F_{link} = \frac{(1+(T_{bath}/T_c)^{n+1})}{2}. \quad (2)$$

The spectral density of the Johnson noise from the shunt resistance is $4k_B T_{bath} R_{sh}$, while the TES Johnson noise term is $4k_B T_c R_0 J_{excess}$, where J_{excess} is a factor required to account for excess high-frequency noise in the measured noise spectra. Irwin [8] predicts $J_{excess} \approx 1+2\beta$ for $\beta << 1$. The best fit values for J_{excess} at each setpoint are listed in Table 2 and are seen to agree with that limiting case.

RESULTS

Table 2 tabulates the fitted parameters for the two TESes on one polarimeter (labeled TESA and TESB) from the two-block model and also lists the noise equivalent power (NEP) at 10 Hz, estimated by dividing the measured noise spectrum by the predicted responsivity. The parameters C_1, C_2 and G_2 from the two devices agree to within the measurement errors of 25% ; however C_1+C_2 is about six times larger than initial predictions. We note, however, that Rostem et al [9] measured heat capacities approximately 20 times larger than the bulk value for thin films of SiN which may be a clue to these results.

Figure 2 plots the $Z(\omega)$ fits for the two- and three-block models applied to TESA, along with the data. The lower panels overlay the measured noise spectra at one setpoint with predictions from each of the models. Note that we use a linear scale for the noise ordinate axis: the data agree well with predictions from both models. The two-block model does not capture all the high signal-to-noise features in $Z(\omega)$; adding a third thermal block does significantly better. Moreover, the noise predictions from the three-block model are substantially better than from the two-block model in the 5-50 Hz range that is crucial for most CMB measurements. We note, however, that fits from other simple three-block models, such as one in which all three blocks are in series, result in comparable improvements. Though we only show the noise for one setpoint for clarity, we draw the same conclusions from the other two setpoints, and from the data from the second TES.

Future goals are to better understand the heat capacity discrepancy, to identify thermal blocks with distinct bolometer components, and to extend this analysis to the dozens of polarimeters we have fabricated so far, which have several discrete values of T_c and G [**?**].

ACKNOWLEDGEMENTS

Work at the University of Chicago is supported by the National Science Foundation through grant ANT-0638937 and the NSF Physics Frontier Center grant PHY-0114422 to the Kavli Institute of Cosmological Physics at the University of Chicago. It also receives generous support from the Kavli Foundation and the Gordon and Betty Moore Foundation. Work at NIST is supported by the NIST Innovations in Measurement Science program. Work at the University of Colorado is supported by the National Science Foundation through grant AST-0705302. Work at Princeton University is supported by the National Science Foundation through grant PHY-0355328 and grant ???. It also received support from Princeton University start-up funds

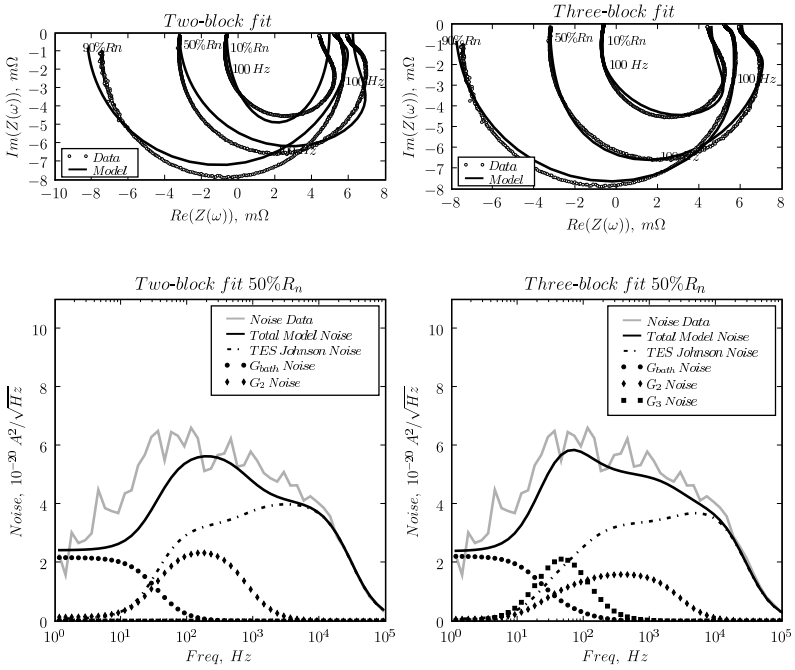

FIGURE 2. This figure contains data from TESB operating at T_{bath}=320 mK. The complex impedance data shown in the first row of plots were obtained using the swept sine method. The first column of plots corresponds to the two-block model; the second column corresponds to the three-block model. For each $Z(\omega)$ curve the 100 Hz label is printed near $Z(2\pi\ 100\ Hz)$. $Z(\omega)$ at 10% R_n is the hardest setpoint to fit because its high loop gain moves the high frequency bends to the middle of the $Z(\omega)$ curve. Note that the shunt Johnson noise does not appear in the second row of plots because it is negligible at 50% R_n.

REFERENCES

1. K. D. Irwin, and G. C. Hilton, "Transition Edge Sensors," in *Cryogenic Particle Detection*, edited by C. Enss, Springer-Verlag Berlin Heidelberg, 2005.
2. M. Galeazzi, and D. McCammon, *J. Appl. Phys.* **93**, 4856–4869 (2003).
3. E. Figueroa-Feliciano, *Theory and development of position-sensitive quantum calorimeters*, Ph.D. thesis, Stanford University (2001).
4. C. Kittel, and H. Kroemer, *Thermal Physics*, Freeman, 1980.
5. W. Holmes, J. Gildemeister, P. Richards, and V. Kotsubo, *Applied physics letters* **72**, 2250–2 (1998).
6. M. Meissner, and P. Strehlow, *Journal of Low Temperature Physics* **137**, 355–69 (2004).
7. J. C. Mather, *Appl. Opt.* **21**, 1125–1129 (1982).
8. K. Irwin, *Nuclear Instruments and Methods in Physics Research Section A: Accelerators, Spectrometers* **559**, 718–720 (2006).
9. K. Rostem, D. Glowacka, D. Goldie, and S. Withington, *Proc. SPIE* **7020**, 70200L (2008).